

# OBLIQUITY AND ECCENTRICITY CONSTRAINTS FOR TERRESTRIAL EXOPLANETS

STEPHEN R. KANE<sup>1,2</sup>, STEPHANIE M. TORRES<sup>2</sup>

<sup>1</sup>Department of Earth Sciences, University of California, Riverside, CA 92521, USA

<sup>2</sup>Department of Physics & Astronomy, San Francisco State University, 1600 Holloway Avenue, San Francisco, CA 94132, USA

## ABSTRACT

Exoplanet discoveries over recent years have shown that terrestrial planets are exceptionally common. Many of these planets are in compact systems that result in complex orbital dynamics. A key step toward determining the surface conditions of these planets is understanding the latitudinally dependent flux incident at the top of the atmosphere as a function of orbital phase. The two main properties of a planet that influence the time-dependent nature of the flux are the obliquity and orbital eccentricity of the planet. We derive the criterion for which the flux variation due to obliquity is equivalent to the flux variation due to orbital eccentricity. This equivalence is computed for both the maximum and average flux scenarios, the latter of which includes the effects of the diurnal cycle. We apply these calculations to four known multi-planet systems (GJ 163, K2-3, Kepler-186, and Proxima Centauri), where we constrain the eccentricity of terrestrial planets using orbital dynamics considerations and model the effect of obliquity on incident flux. We discuss the implications of these simulations on climate models for terrestrial planets and outline detectable signatures of planetary obliquity.

*Keywords:* astrobiology – planetary systems – stars: individual (GJ 163, K2-3, Kepler-186, Proxima Centauri)

## 1. INTRODUCTION

Exoplanetary science is rapidly requiring the need for characterization techniques for terrestrial planets as their discovery rate continues to increase. The *Kepler* mission has demonstrated that planet frequency increases with smaller size (Fressin et al. 2013; Howard 2013; Petigura et al. 2013), implying that the *Transiting Exoplanet Survey Satellite* will discover numerous examples of terrestrial planets around bright host stars (Ricker et al. 2015; Sullivan et al. 2015). Significant attention is given to those planets that lie within the Habitable Zone (HZ) of their host stars (Kasting et al. 1993; Kopparapu et al. 2013, 2014), although the HZ is primarily a target selection tool for future atmospheric studies (Kane & Gelino 2012a). In the meantime, General Circulation Models (GCMs) are used to provide our best estimate of the surface conditions for discovered HZ planets (Wordsworth et al. 2010, 2011; Leconte et al. 2013; Wolf & Toon 2013; Yang et al. 2013; Wolf & Toon 2014; Yang et al. 2014; Leconte et al. 2015; Kopparapu et al. 2016).

A primary driving force in GCMs affecting surface conditions, climate dynamics, and seasonal variations,

is the instellation flux on the planet (Kaspi & Showman 2015). Two primary factors effect the variability of the instellation flux: orbital eccentricity and obliquity. Tidal effects can occasionally play a significant role for planets in eccentric orbits and/or involved in planet-planet interactions (Barnes et al. 2008, 2009) and may even push the planet into a runaway greenhouse scenario (Barnes et al. 2013; Driscoll & Barnes 2015). The effect of eccentricity on planetary atmospheres and subsequent climate variations follows a Keplerian pattern of long winters interrupted by brief periods of “flash heating” during periastron passage (Williams & Pollard 2002; Dressing et al. 2010; Kane & Gelino 2012b; Bolmont et al. 2016). The obliquity of a planet’s rotational axis undergoes short and long term oscillations due to perturbations from other planetary bodies in the system (Laskar 1986). Fluctuations in planetary obliquity can have large effects on climates (Williams & Kasting 1997) and extreme obliquities can move the outer edge of the HZ (Williams & Pollard 2003; Armstrong et al. 2014; Linsenmeier et al. 2015). Of the two primary factors, orbital eccentricity is currently a far more accessible measurable than obliquity. However, for systems in which we have constraints on eccentricity, we can determine the range of obliquities that drive the variation of instellation flux.

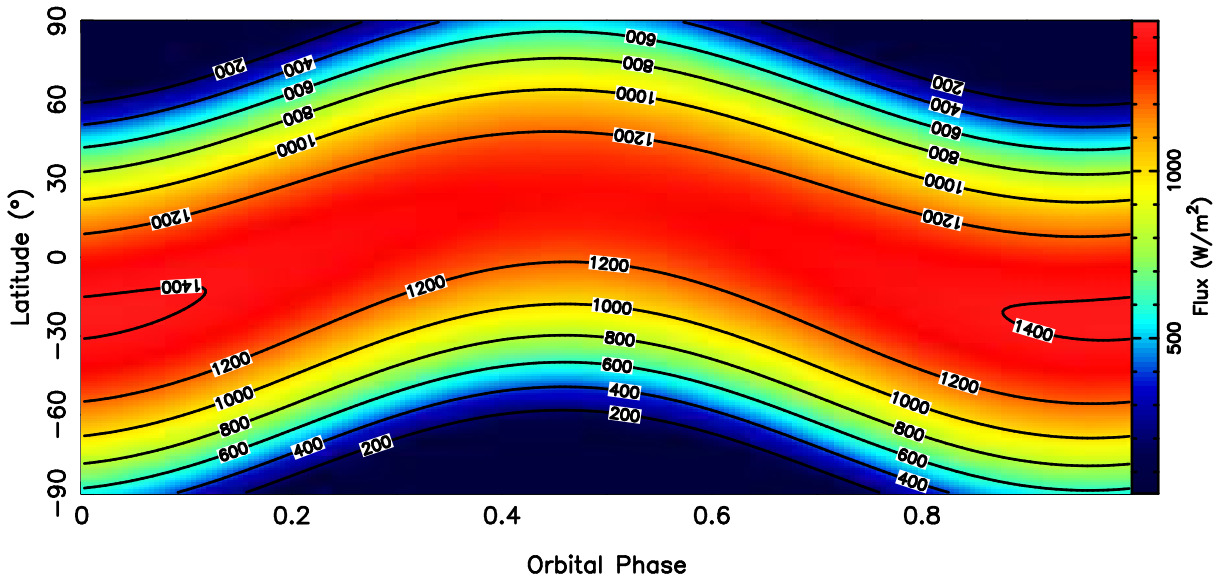


**Figure 1.** A map of the maximum incident flux received by an Earth analog as a function of latitude and phase. The phase of  $\phi = 0.0$  corresponds to periastron passage of the planet.

Here, we describe the latitudinal flux incident on an exoplanet as a function of obliquity, eccentricity, and orbital phase. We further show how eccentricity constraints from radial velocity (RV) measurements or dynamical constraints can be used to model obliquity-dependent flux variations and locate regions where the changes in flux due to obliquity are equivalent to those due to eccentricity. In Section 2 we formulate the time variable flux and equate regions of flux change in obliquity and eccentricity parameter space, both for maximum and average flux scenarios. In Section 3 we provide stability criteria for known terrestrial planets in the GJ 163, K2-3, Kepler-186, and Proxima Centauri systems and model their potential flux maps as a function of obliquity. In Section 4 we discuss the implications of the flux variations for surface temperatures and atmospheric conditions in so far as they effect habitability. We provide concluding remarks and suggestions for future work in Section 5.

## 2. THE TIME VARIABLE FLUX

Here, we consider the orbital eccentricity and the obliquity of the planetary rotation axis as sources of variable flux as a function of latitude. For a given eccentricity,  $e$ , semi-major axis,  $a$ , and star-planet separation,  $r$ , the maximum flux occurs at periastron,  $r = a(1 - e)$ , and the minimum flux occurs at apastron,  $r = a(1 + e)$ . In Section 2.1, we calculate maximum incident flux (when the star crosses the local meridian) for a given latitude. This maximum flux can be considered the instantaneous flux, or the latitudinal flux received as a planet nears synchronous rotation (tidal locking). In Section 2.2, we calculate the average the flux over the diurnal cycle of

the planet, which applies to planets whose rotation period is significantly smaller than the orbital period.

### 2.1. Maximum Flux Variation

The maximum flux at latitude  $\beta$  is given by

$$\begin{aligned} F &= \frac{L_\star}{4\pi r^2} (\sin \delta \sin \beta + \cos \delta \cos \beta) \\ &= \frac{L_\star}{4\pi r^2} \cos |\beta - \delta| \end{aligned} \quad (1)$$

where  $L_\star$  is the stellar luminosity. The solar declination,  $\delta$ , is given by:

$$\delta = \theta \cos[2\pi(\phi - \Delta\phi)] \quad (2)$$

for which  $\phi$  is the orbital phase,  $\Delta\phi$  is the offset in phase between periastron and highest solar declination in the northern hemisphere, and  $\theta$  is the obliquity. For the Earth,  $\Delta\phi = 0.46$  and  $\theta = 23.5^\circ$ . Figure 1 is an incident flux map for an Earth-Sun analog as a function of latitude with contours of constant flux throughout a complete orbital phase. The phase of  $\phi = 0.0$  corresponds to the planet's periastron passage.

The aim of the calculations here is to determine values of  $e$  and  $\theta$  where the maximum change in flux during an orbit,  $\Delta F$ , are equivalent at a given latitude,  $\beta$ . For the change in flux due to  $e$ , we assume  $\theta = 0^\circ$ , and likewise for the change in flux due to  $\theta$ , we assume  $e = 0$ . For eccentricity, the maximum change in flux is the difference in flux between periastron and apastron:

$$\begin{aligned} \Delta F_e &= \frac{L_\star}{4\pi a^2(1 - e)} \cos \beta - \frac{L_\star}{4\pi a^2(1 + e)} \cos \beta \\ &= \frac{L_\star}{4\pi a^2} \cos \beta \left( \frac{1}{1 - e} - \frac{1}{1 + e} \right) \end{aligned}$$

$$= \frac{L_\star}{2\pi a^2} \frac{e}{(1-e^2)} \cos \beta \quad (3)$$

For obliquity, the maximum change in flux occurs amidst the difference between the minimum and maximum solar declination. When  $\theta \leq 45^\circ$  and  $\theta \leq \beta \leq 90^\circ - \theta$ , this can be expressed as:

$$\begin{aligned} \Delta F_\theta &= \frac{L_\star}{4\pi a^2} \cos(\beta - \theta) - \frac{L_\star}{4\pi a^2} \cos(\beta + \theta) \\ &= \frac{L_\star}{4\pi a^2} [\cos(\beta - \theta) - \cos(\beta + \theta)] \\ &= \frac{L_\star}{2\pi a^2} \sin \beta \sin \theta \end{aligned} \quad (4)$$

For  $\beta < \theta$ , the following applies:

$$\Delta F_\theta = \frac{L_\star}{4\pi a^2} [1 - \cos(\beta + \theta)] \quad (5)$$

and for  $\beta > 90^\circ - \theta$ , the following applies:

$$\Delta F_\theta = \frac{L_\star}{4\pi a^2} \cos(\beta - \theta) \quad (6)$$

Thus, the maximum flux changes due to eccentricity and obliquity are equivalent where  $\Delta F_e = \Delta F_\theta$ . Solving for obliquity in the regime  $\theta \leq \beta \leq 90^\circ - \theta$ , we combine Equations 3 and 4:

$$\begin{aligned} \frac{L_\star}{2\pi a^2} \frac{e}{(1-e^2)} \cos \beta &= \frac{L_\star}{2\pi a^2} \sin \beta \sin \theta \\ \frac{e}{(1-e^2)} &= \tan \beta \sin \theta \\ \theta &= \arcsin \left[ \frac{e}{(1-e^2) \tan \beta} \right] \end{aligned}$$

For  $\beta < \theta$ , we combine Equations 3 and 5:

$$\begin{aligned} \frac{L_\star}{2\pi a^2} \frac{e}{(1-e^2)} \cos \beta &= \frac{L_\star}{4\pi a^2} [1 - \cos(\beta + \theta)] \\ \frac{e}{(1-e^2)} &= \frac{1 - \cos(\beta + \theta)}{2 \cos \beta} \\ \theta &= \arccos \left[ 1 - 2 \cos \beta \frac{e}{(1-e^2)} \right] - \beta \end{aligned}$$

For  $\beta > 90^\circ - \theta$ , we combine Equations 3 and 6:

$$\begin{aligned} \frac{L_\star}{2\pi a^2} \frac{e}{(1-e^2)} \cos \beta &= \frac{L_\star}{4\pi a^2} \cos(\beta - \theta) \\ \frac{e}{(1-e^2)} &= \frac{\cos(\beta - \theta)}{2 \cos \beta} \\ \theta &= \beta - \arccos \left[ 2 \cos \beta \frac{e}{(1-e^2)} \right] \end{aligned}$$

Solving for eccentricity results in:

$$e = \frac{\sqrt{1 + f(\theta, \beta)^2} - 1}{f(\theta, \beta)} \quad (7)$$

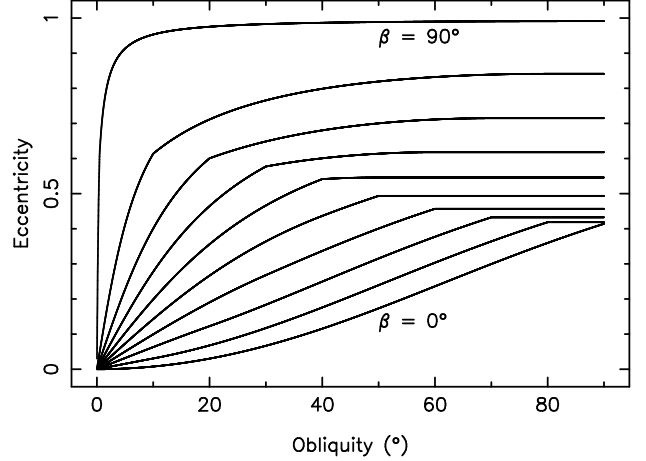


**Figure 2.** Orbital eccentricity as a function of the obliquity of the rotational axis. The lines of constant latitude represent equivalence of flux variation received ( $\Delta F_e = \Delta F_\theta$ ) during one complete orbital period.

where the function  $f(\theta, \beta)$  for  $\theta \leq 45^\circ$  is given by:

$$f(\theta, \beta) = \begin{cases} 2 \tan \beta \sin \theta & \text{for } \theta \leq \beta \leq 90^\circ - \theta \\ \frac{1 - \cos(\beta + \theta)}{\cos \beta} & \text{for } \beta < \theta \\ \frac{\cos(\beta - \theta)}{\cos \beta} & \text{for } \beta > 90^\circ - \theta \end{cases} \quad (8)$$

Equations 7 and 8 allow the calculation of orbital eccentricities for which the total change in incident flux is the same as obliquities with  $\theta \leq 45^\circ$ . Using the same methodology for  $\theta > 45^\circ$ , the function  $f(\theta, \beta)$  is given by:

$$f(\theta, \beta) = \begin{cases} \frac{1}{\cos \beta} & \text{for } \theta \geq \beta \geq 90^\circ - \theta \\ \frac{1 - \cos(\beta + \theta)}{\cos \beta} & \text{for } \beta < 90^\circ - \theta \\ \frac{\cos(\beta - \theta)}{\cos \beta} & \text{for } \beta > \theta \end{cases} \quad (9)$$

Shown in Figure 2 are the locations of eccentricity and obliquity where the flux variation during a complete orbital phase are equivalent to each other. We plot this for latitudes ranging from  $\beta = 0^\circ$  to  $\beta = 90^\circ$  in steps of  $10^\circ$ . At latitudes close to the poles, the variation between winter and summer incident flux increases as the pole is tilted toward the ecliptic plane. The minimum flux for an eccentric orbit  $e < 1$  will never reach zero, even at apastron. Thus, an obliquity of  $\theta = 90^\circ$  approaches a boundary condition where the flux difference is equivalent to that of a hyperbolic orbit.

There is a difference that should be noted for the change in flux due to eccentricity and obliquity. Although the flux variation due to obliquity at a given latitude varies sinusoidally, the flux variation due to eccentricity varies based on the star-planet separation produced by a Keplerian orbit. Therefore, though the total change in flux is the same, the rate at which the flux varies between minimum and maximum are differ-

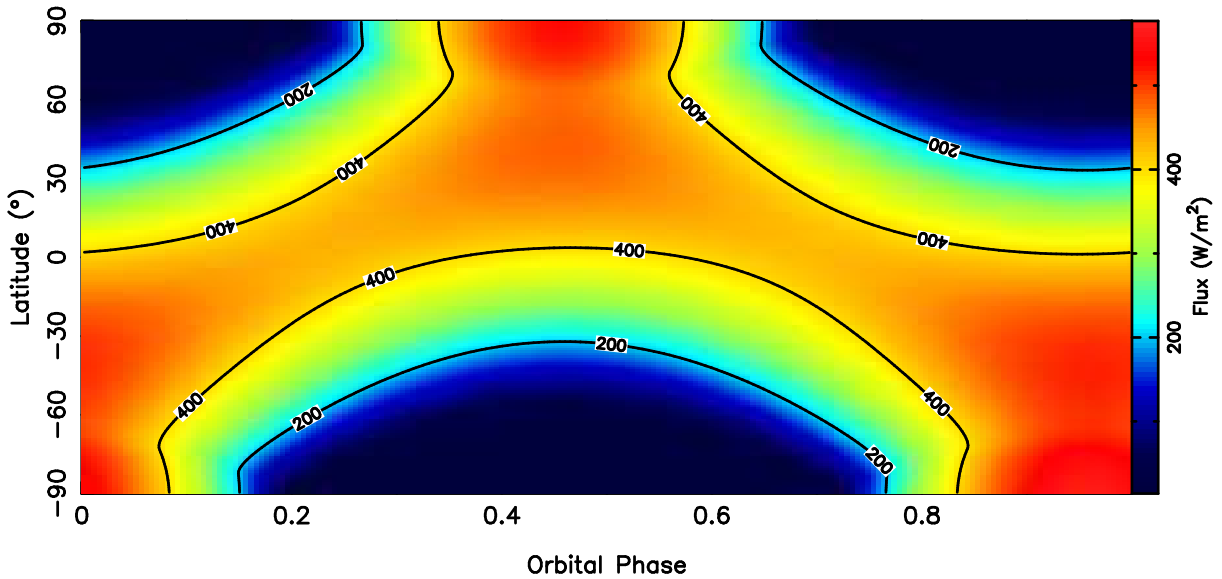


**Figure 3.** A map of the incident flux received by an Earth analog, averaged over the diurnal cycle, as a function of latitude and phase. The phase of  $\phi = 0.0$  corresponds to periastron passage of the planet.

ent for the eccentricity and obliquity scenarios, likely resulting in a different atmospheric response over the orbital phase time scale.

### 2.2. Diurnal Cycle Effects

For planets where the rotation period is significantly less than the orbital period, the average incident flux as a function of latitude may be used. For this purpose, Equation 1 is modified as follows

$$F = \frac{L_{\star}}{4\pi r^2} (\sin \delta \sin \beta + \cos \delta \cos \beta \cos h) \quad (10)$$

where  $h$  is the hour angle of the star with respect to the local meridian. The fraction of planetary rotation period that experiences daylight for a given latitude is

$$\Delta t_{dl} = \frac{2 \arccos(-\tan \delta \tan \beta)}{360^{\circ}} \quad (11)$$

For obliquities of  $\theta > 0^{\circ}$ , there will be latitudes that experience constant day/night during the course of an orbital period. These situations are defined by the criteria that if  $\beta + \delta > 90^{\circ}$  or  $\beta + \delta < -90^{\circ}$  then  $\Delta t_{dl} = 1.0$ , and if  $\beta - \delta > 90^{\circ}$  or  $\beta - \delta < -90^{\circ}$  then  $\Delta t_{dl} = 0.0$ . The average flux at a given latitude can then be calculated by accounting for the change in flux as a function of  $h$  and the fractional daylight time. Figure 3 is an incident flux map averaged over the diurnal cycle for an Earth–Sun analog as a function of latitude. The comparison with Figure 1 shows the impact of including the effect of constant daylight periods on the polar regions.

As for Section 2.1, we now calculate the values of  $e$  and  $\theta$  where the change in the average flux during an orbit,  $\Delta F$ , are equivalent at a given latitude,  $\beta$ . For the eccentricity case with  $\theta = 0^{\circ}$ , the average flux is equiv-

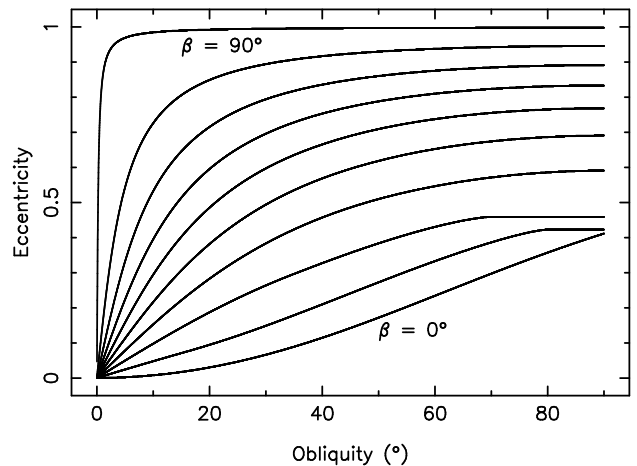


**Figure 4.** As for Figure 2, this figure shows the orbital eccentricity as a function of the obliquity of the rotational axis, but now includes the effect of the diurnal cycle. The lines of constant latitude represent equivalence of flux variation received ( $\Delta F_e = \Delta F_{\theta}$ ) during one complete orbital period.

alent to the amplitude shown in Equation 3 multiplied by the average of a sine function including the effect of a day/night cycle. This leads to an additional  $1/\pi$  factor, as follows

$$\Delta F_e = \frac{L_{\star}}{2\pi^2 a^2} \frac{e}{(1 - e^2)} \cos \beta \quad (12)$$

For obliquity, the introduction of the hour angle and fraction daylight in Equations 10 and 11 produce a non-trivial calculation of  $\Delta F_{\theta}$  for various obliquity and latitude ranges. We solve this by numerically calculating regions where  $\Delta F_e = \Delta F_{\theta}$ . The result of these calculations are summarized in Figure 4 where, as for Figure 2, we plot lines of constant latitude from  $\beta = 0^{\circ}$  to  $\beta = 90^{\circ}$

in steps of  $10^\circ$ . The main effect of including the diurnal cycle is to smooth the relationship with eccentricity due to the averaging of the flux received for a given latitude. Additionally, the diurnal cycle increases the equivalent eccentricity at high latitudes, as the change in average flux is larger than for the maximum flux case described in Section 2.1. The combination of the two factors, eccentricity and obliquity, are investigated for specific planets in the case studies that follow.

### 3. CASE STUDIES

Here, we apply eccentricity constraints through stability considerations to four of the known exoplanets: GJ 163 c, K2-3 d, Kepler-186 f, and Proxima Centauri b. These are then used to determine latitudinal flux maps of the planets as a function of orbital phase for fixed obliquities, including diurnal effects. The four exoplanets were carefully chosen from the known terrestrial exoplanets considering their proximity to the HZ and the diversity of the system architectures. System parameters were extracted from the NASA Exoplanet Archive (Akeson et al. 2013) and relevant publications (see Table 1).

**Table 1.** Stellar and Planetary Parameters

Parameter	GJ 163 c <sup>a</sup>	K2-3 d <sup>b</sup>	Kepler-186 f <sup>c</sup>	Proxima Centauri b <sup>d</sup>
Star				
Spectral Type	M3.5 V	M0.0 V	M1 V	M5.5 V
$V$	$11.811 \pm 0.012$	$12.17 \pm 0.01$	15.65	11.13
Distance (pc)	$15.0 \pm 0.4$	$45 \pm 3$	$151 \pm 18$	1.295
$T_{\text{eff}}$ (K)	$3500 \pm 100$	$3896 \pm 189$	$3788 \pm 54$	$3050 \pm 100$
$M_\star$ ( $M_\odot$ )	$0.40 \pm 0.02$	$0.60 \pm 0.09$	$0.478 \pm 0.055$	$0.120 \pm 0.015$
$R_\star$ ( $R_\odot$ )	–	$0.56 \pm 0.07$	$0.472 \pm 0.052$	$0.141 \pm 0.021$
$L_\star$ ( $L_\odot$ )	$0.0196 \pm 0.001$	$0.065^e$	$0.0412 \pm 0.069$	$0.00155 \pm 0.00006$
CHZ (AU)	$0.145\text{--}0.282^e$	$0.262\text{--}0.500^e$	$0.21\text{--}0.40^e$	$0.041\text{--}0.081^e$
OHZ (AU)	$0.115\text{--}0.297^e$	$0.207\text{--}0.527^e$	$0.17\text{--}0.42^e$	$0.032\text{--}0.086^e$
Planet				
$P$ (days)	$25.63 \pm 0.03$	$44.5631^{+0.0063}_{-0.0055}$	$129.9459 \pm 0.0012$	$11.186 \pm 0.002$
$e$	$0.099 \pm 0.086$	$< 0.162^e$	$< 0.628^e$	$< 0.35$
$\omega$ ( $^\circ$ )	$227 \pm 80$	–	–	310
$M_p$ ( $M_\oplus$ )	$6.8 \pm 0.9$	$3.97^e$	$1.54^e$	$1.27^{+0.19}_{-0.17}$
$R_p$ ( $R_\oplus$ )	–	$1.52^{+0.21}_{-0.20}$	$1.11^{+0.14}_{-0.13}$	–
$a$ (AU)	$0.1254 \pm 0.0001$	$0.2076^{+0.0098}_{-0.0108}$	$0.356 \pm 0.048$	$0.0485^{+0.0051}_{-0.0041}$
$R_H$ (AU)	–	$0.004^e$	$0.005^e$	–

<sup>a</sup>Bonfils et al. (2013); Tuomi & Anglada-Escudé (2013)

<sup>b</sup>Crossfield et al. (2015)

<sup>c</sup>Quintana et al. (2014)

<sup>d</sup>Anglada-Escudé et al. (2016)

<sup>e</sup>Calculated in this work.

#### 3.1. Stability Criteria

Of the four systems considered here, two were discoveries using the RV technique (GJ 163 and Proxima Centauri). The planets in these systems have measurements and subsequent constraints placed upon their orbital ec-

centricities from the Keplerian fit to the RV data. The remaining two systems, K2-3 and Kepler-186, were detected using the transit method with scant RV data obtained. These two systems thus have limited information available for the planetary orbital eccentricities. Obser-

vations of compact Kepler systems indicate that such planets are likely to be in circular orbits (Kane et al. 2012; Van Eylen & Albrecht 2015). However, here we use stability considerations to determine the maximum eccentricities allowed for planets in those systems.

We use a similar methodology for orbital stability to that used by Crossfield et al. (2015) and Sinukoff et al. (2016). The masses of the transiting planets ( $M_p$ ) were calculated using the mass-radius relationships of Weiss & Marcy (2014). For two-planet systems, a criterion for stability was numerically estimated by Gladman (1993), requiring that the separation of the planets exceed about 3.5 mutual Hill radii ( $R_{H,M_p}$ ), given by

$$R_{H,M_p} = \left[ \frac{M_{p,in} + M_{p,out}}{3M_\star} \right]^{\frac{1}{3}} \frac{(a_{in} + a_{out})}{2} \quad (13)$$

where  $M_\star$  is the mass of the host star and the “in/out” subscripts refer to the inner and outer planets in the system. For multi-planet systems, a long-term stability criterion established by Smith & Lissauer (2009) requires that  $\Delta > 9$  for adjacent planets where  $\Delta = (a_{out} - a_{in})/R_H$ . For three adjacent planets, the criterion becomes  $\Delta_{in} + \Delta_{out} > 18$ , where  $\Delta_{in}$  and  $\Delta_{out}$  are the  $\Delta$  calculations for the inner and outer adjacent planet pairs respectively. By modifying Equation 13 with a  $(1 - e)$  multiplicative factor to account for eccentricity, we are able to determine eccentricities that satisfy the above stability criteria. The results of these calculations for individual systems are described in the sections specific to those systems below.

### 3.2. Habitable Zone

To calculate the HZ boundaries of the four planetary systems studied here, we use the methodology described by Kopparapu et al. (2013, 2014). There are two inner and two outer boundaries calculated, the extent of which depend on assumptions regarding how long Venus and Mars were able to retain liquid water at their surfaces. These are referred to as the Conservative Habitable Zone (CHZ) and the Optimistic Habitable Zone (OHZ), for which a detailed description can be found in Kopparapu et al. (2013). Our calculations for the CHZ and OHZ boundaries for each of the systems are shown in Table 1.

Figure 5 shows a top-down view of the systems, including the planetary orbits and the CHZ (light-green) and OHZ (dark-green) regions. The size along a panel side (scale) in the figure is indicated in the top-right corner of each panel. The parameters used to plot the planetary orbits are those from Table 1 and the associated references. For K2-3 d and Kepler-186 f, we have used the maximum eccentricities for those planets using the calculations of Section 3.1 and described further in Sections 3.4 and 3.5. The percentage of a complete orbital

period spent within the OHZ for each of the four planets are 86% (GJ 163 c), 56% (K2-3 d), 33% (Kepler-186 f), and 94% (Proxima Centauri b).

### 3.3. GJ 163

The known planets orbiting the low-mass star GJ 163 were discovered by Bonfils et al. (2013). Their analysis of the RV data indicated the presence of five periodic signals, two of which were attributed to possible stellar activity sources. The three-planet solution includes a 6.8  $M_{oplus}$  planet (planet c) in a  $\sim 25$  day period orbit. We adopt this three-planet solution and use the stellar parameters of Bonfils et al. (2013) and Tuomi & Anglada-Escudé (2013), as shown in Table 1.

The Keplerian orbit of planet c reveals an orbital eccentricity of  $e \sim 0.1$  which we utilize in our models. According to Figure 2, an obliquity of  $\theta = 16^\circ$  produces an equivalent flux variation to that produced by the  $e = 0.1$  eccentricity at a latitude of  $\beta = 20^\circ$ . For a circular orbit ( $e = 0.0$ ), the maximum flux received by planet c would be  $1705 \text{ W m}^{-2}$  ( $1.25 F_\oplus$ ). Using the measured eccentricity, the maximum flux (during periastron passage) is  $2100 \text{ W m}^{-2}$  ( $1.54 F_\oplus$ ).

Shown in Figure 6 are three incident flux maps for the planet GJ-163 c. As with Figure 1, the flux maps are a function of latitude and orbital phase with contours of constant flux. The phase of  $\phi = 0.0$  corresponds to the planet’s periastron passage. All three panels use the known eccentricity of  $e = 0.099$ . The top panel assumes an obliquity of  $\theta = 20^\circ$  and a phase offset between periastron and highest stellar declination in the northern hemisphere of  $\Delta\phi = 0.0$ . The lower two panels assume  $\Delta\phi = 0.25$  and obliquities of  $\theta = 50^\circ$  (middle) and  $\theta = 80^\circ$  (bottom). Choosing  $\Delta\phi = 0.25$  demonstrates the effect of decoupling the incident flux effects of periastron and maximum stellar declination in a particular hemisphere. Using the methodology of Section 2.2, the eccentricity of  $e \sim 0.1$  and obliquity of  $\theta = 20^\circ$  have approximately equivalent effects on the seasonal variations in flux at low latitudes, and thus supply similar driving energy for the climate variations in those low latitude regions. The middle and bottom panels of Figure 6 show that the obliquity becomes the dominant source of variable energy for  $\theta > 20^\circ$ , with a mean incident flux of  $0.98 F_\oplus$  in the latitude range of  $-30^\circ > \beta > +30^\circ$  for  $\theta = 50^\circ$ .

### 3.4. K2-3

An early result from the K2 mission (Howell et al. 2014) was the discovery of the planetary system K2-3 by Crossfield et al. (2015). The system parameters were subsequently refined further by the work of Almenara et al. (2015) and Sinukoff et al. (2016). The stellar and planetary properties shown in Table 1 are

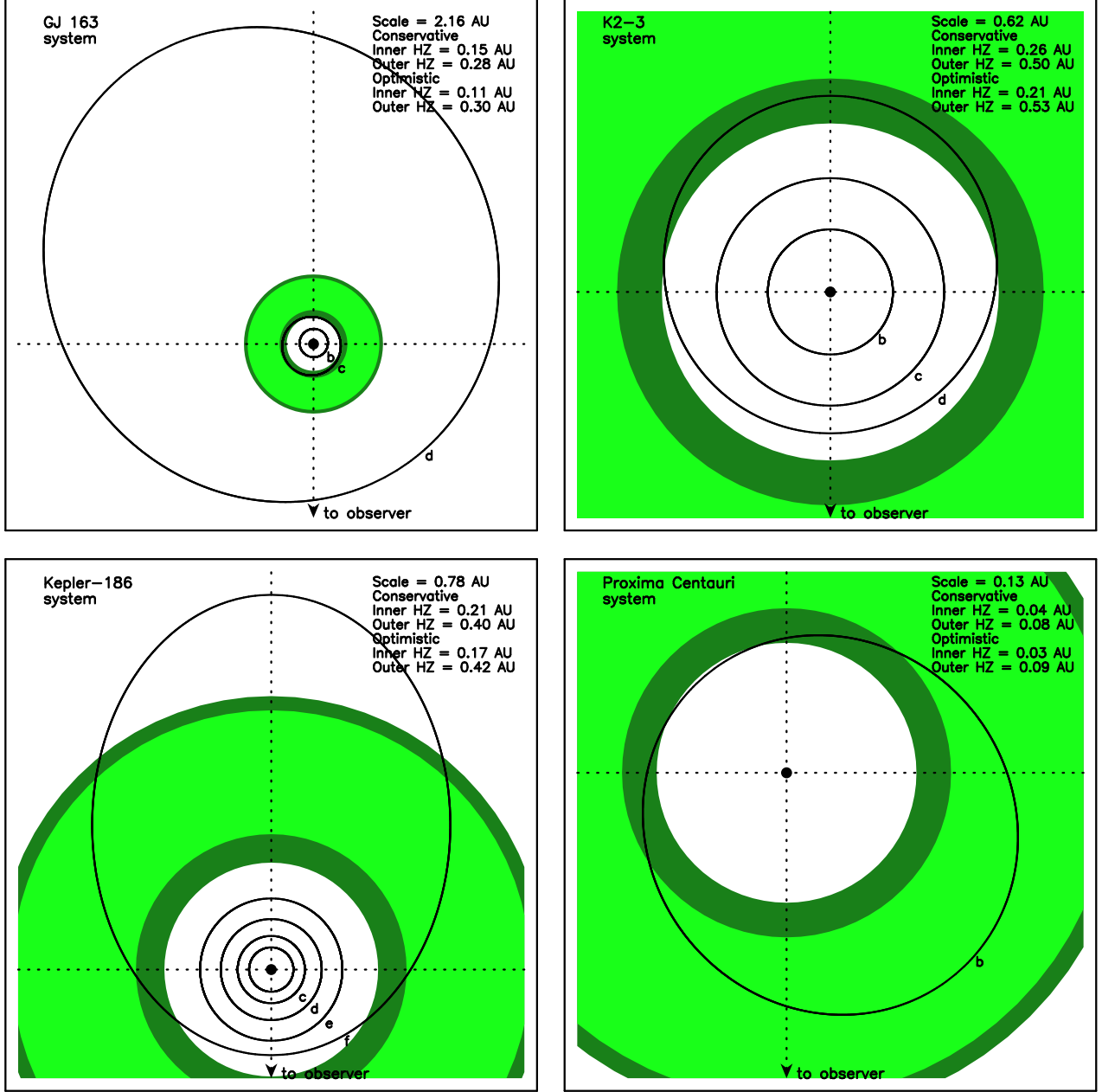


**Figure 5.** Top-down views of the GJ-163 (top-left), K2-3 (top-right), Kepler-186 (bottom-left), and Proxima Centauri (bottom-right) systems. The orbits of the planets are shown overlaid on the conservative (light-green) and optimistic (dark-green) HZ regions. The size along a panel side (scale) is indicated in the top-left corner of each panel. For K2-3 d and Kepler-186 f, the orbital eccentricities adopted are the maximum allowed from stability arguments (see Table 1 and Section 3.1).

those from [Crossfield et al. \(2015\)](#), as they provide a self-consistent model of the system. Using the stability criteria described in Section 3.1, we calculated the estimated planet mass and subsequent limits on the orbital eccentricity of the outermost planet known in the system, planet d. For a circular orbit, the semi-major axis of planet d corresponds to the inner edge of the OHZ and the Hill radius is 0.004 AU (see Table 1). By adjusting the eccentricity of the planet, the limit

of  $\Delta \sim 9$  is reached at an eccentricity of  $e = 0.162$  where the mutual Hill radius for the outer two planets is  $R_{H,M_p} = 0.004$  AU. Adopting this eccentricity for the outer planet results in an orbital architecture that is depicted in the top-right panel of Figure 5, where planet d enters the OHZ during apastron. Although we have selected an argument of periastron of  $\omega = 90^\circ$ , the value of  $\omega$  has no impact on our flux calculations and the transit duration will provide limits on the allowed perias-

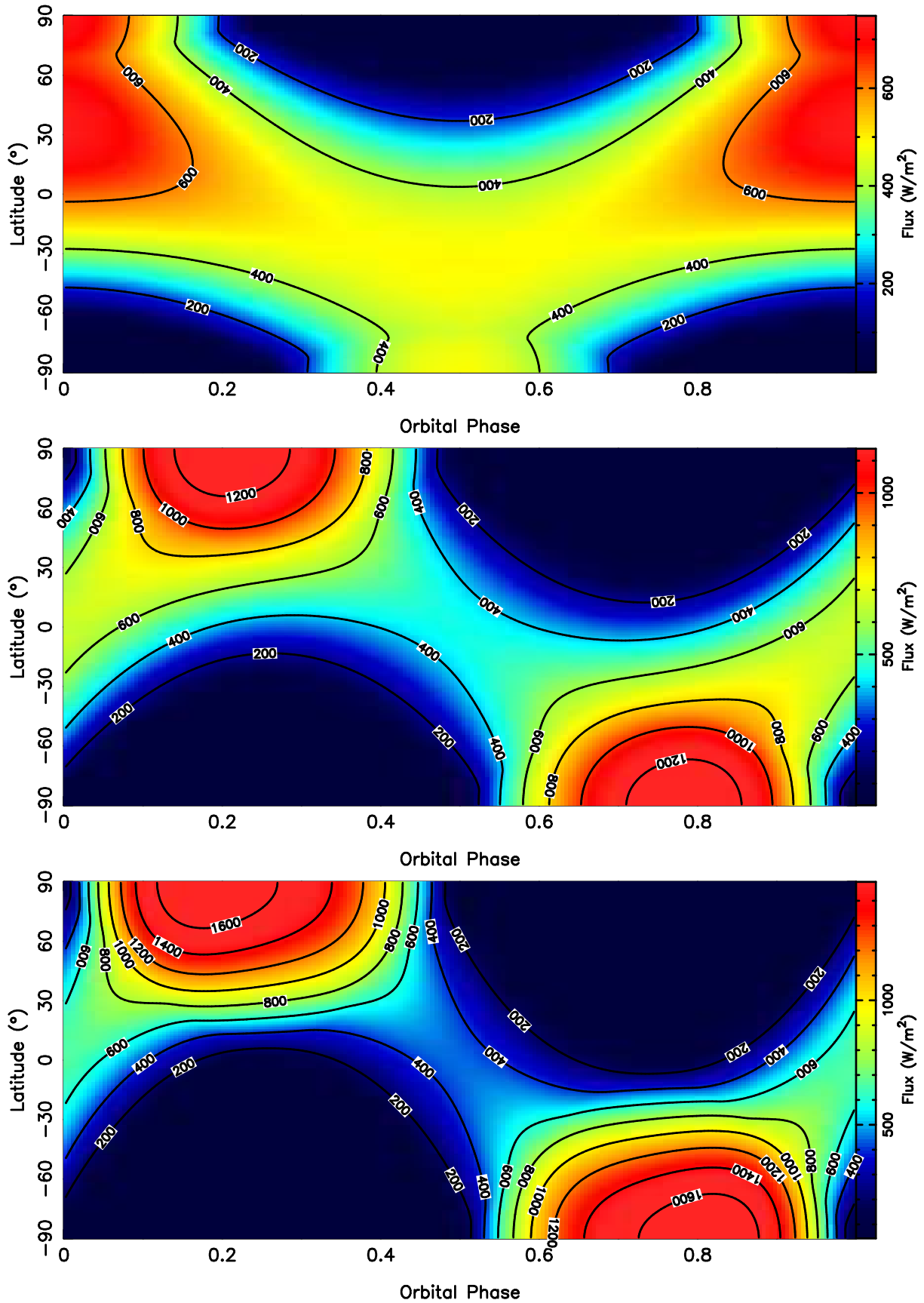


**Figure 6.** Incident flux intensity maps of the planet GJ-163 c as a function of latitude and orbital phase, where phase  $\phi = 0.0$  corresponds to periastron passage of the planet. Top:  $e = 0.099$ ,  $\theta = 20^\circ$ ,  $\Delta\phi = 0.0$ . Middle:  $e = 0.099$ ,  $\theta = 50^\circ$ ,  $\Delta\phi = 0.25$ . Bottom:  $e = 0.099$ ,  $\theta = 80^\circ$ ,  $\Delta\phi = 0.25$ .



tron values for a given eccentricity (Kane & von Braun 2008).

From Figure 4, it can be seen that the eccentricity of  $e = 0.162$  results in an equivalent flux variation to an obliquity of  $\theta = 17^\circ$  at a latitude of  $\beta = 20^\circ$ . If planet d is in a circular orbit, the flux received by the planet during the entire orbit is  $2055 \text{ W m}^{-2}$ , ( $1.50 F_\oplus$ ). For an eccentricity of  $e = 0.162$ , the maximum flux received is  $2925 \text{ W m}^{-2}$  ( $2.14 F_\oplus$ ). Shown in Figure 7 are the flux intensity maps for K2-3 d as a function of latitude and orbital phase where, once again, we include the diurnal effects. The top panel assumes a circular orbit, an obliquity of  $\theta = 20^\circ$ , and  $\Delta\phi = 0.0$ . The bottom two panels assume a maximum eccentricity of  $e = 0.162$ ,  $\Delta\phi = 0.25$ , and obliquities of  $50^\circ$  and  $80^\circ$  for the middle and bottom panels respectively. The amplitude of the flux variation effects in the top panel are below those predicted by the maximum eccentricity and would thus result in a more temperate climate than the eccentric cases in the bottom two panels. The mean incident flux in the latitude range of  $-30^\circ > \beta > +30^\circ$  for  $\theta = 50^\circ$  (Figure 7, middle panel) is  $1.20 F_\oplus$ .

### 3.5. Kepler-186

The multi-planet system, Kepler-186, was confirmed by Lissauer et al. (2014) and Rowe et al. (2014) and later confirmed to have a fifth planet by Quintana et al. (2014). The new outer planet, designated Kepler-186 f, was a particularly important discovery due to its relatively small size and location within the HZ of the host star Bolmont et al. (2014). Our adopted stellar and planetary properties for the Kepler-186 system are from Quintana et al. (2014) and are shown in Table 1. Combining these parameters with the methodology of Section 3.1 results in a maximum eccentricity of the outer planet of  $e = 0.628$  where the mutual Hill radius for the outer two planets is  $R_{H,M_p} = 0.0025 \text{ AU}$ . Adopting this eccentricity for Kepler-186 f results in the orbital architecture depicted in the bottom-left panel of Figure 5. We will explore the effect of this extreme eccentricity limit on flux variations noting that, as for K2-3 d, the periastron argument for an eccentric orbit may be constrained from the transit duration.

As can be seen in Figure 2 and Figure 4, such an extreme eccentricity has no obliquity equivalent at latitude  $\beta = 20^\circ$  regardless of diurnal effects. Such obliquity-induced flux variations are only possible for  $\theta > 60^\circ$  for the maximum flux case and  $\theta > 30^\circ$  for the diurnal case. Planet f is toward the outer edge of the system HZ and, for a circular orbit, receives a maximum flux of  $445 \text{ W m}^{-2}$  ( $0.33 F_\oplus$ ). Adopting the extreme eccentricity of  $e = 0.628$  creates a significant change in this result, with a maximum flux during periastron passage of  $3212 \text{ W m}^{-2}$  ( $2.35 F_\oplus$ ). The flux intensity maps for

Kepler-186 f as a function of latitude and orbital phase using the diurnal model are shown in Figure 8. The top panel shows the flux map for the scenario of a circular orbit, an obliquity of  $\theta = 20^\circ$ , and an alignment of maximum stellar declination and periastron passage ( $\Delta\phi = 0.0$ ). The bottom two panels assume a maximum stellar declination phase offset from periastron passage of  $\Delta\phi = 0.25$ . The middle panel represents the extreme eccentricity scenario with  $e = 0.628$  and an obliquity of  $\theta = 50^\circ$  and further demonstrates how the eccentricity dominates the flux variations for even relatively high obliquities. The scenario shown in the bottom panel assumes a more moderate eccentricity of  $e = 0.3$  where the obliquity of  $\theta = 80^\circ$  is more readily able to drive the seasonal flux variations.

### 3.6. Proxima Centauri

The terrestrial planet orbiting Proxima Centauri was discovered by Anglada-Escudé et al. (2016). This is a naturally high-value planet as it is, by definition, the closest exoplanet to our planetary system. The value is increased by its orbit lying within the HZ of the host star, leading to the exploration of potentially habitable conditions and detectable biosignatures (Barnes et al. 2017; Meadows et al. 2017; Ribas et al. 2016; Turbet et al. 2016). Although they are not entirely ruled out, no evidence of planetary transits have been found at this time (Anglada-Escudé et al. 2016; Davenport et al. 2016). The orbital solution provided by Anglada-Escudé et al. (2016) has a maximum orbital eccentricity of  $e = 0.35$ . Kane et al. (2017) utilized this eccentricity to calculate observable signatures as a function of planet mass, and they also performed stability simulations that exclude the presence of additional terrestrial planets in the HZ of the system. The orbit of the planet in relation to the system HZ is shown in the bottom-right panel of Figure 5, where the maximum eccentricity has been adopted.

According to Figure 4, the maximum eccentricity of  $e = 0.35$  produces a flux variation equivalent to an obliquity of  $\theta = 44^\circ$  at a latitude of  $\beta = 20^\circ$ . For the circular orbit scenario, the maximum flux received by the planet is  $901 \text{ W m}^{-2}$  ( $0.66 F_\oplus$ ), whereas the eccentric scenario results in a maximum incident flux of  $2133 \text{ W m}^{-2}$  ( $1.56 F_\oplus$ ). The flux intensity maps for Proxima Centauri b as a function of latitude and orbital phase are shown in Figure 9. The top panel represents the circular orbit case along with an obliquity of  $\theta = 20^\circ$  and an alignment of maximum stellar declination and periastron passage ( $\Delta\phi = 0.0$ ). The bottom two panels of Figure 9 represent the maximum eccentricity case and assume a maximum stellar declination phase offset from periastron passage of  $\Delta\phi = 0.25$ . The middle panel shows the flux map for an obliquity of  $\theta = 50^\circ$

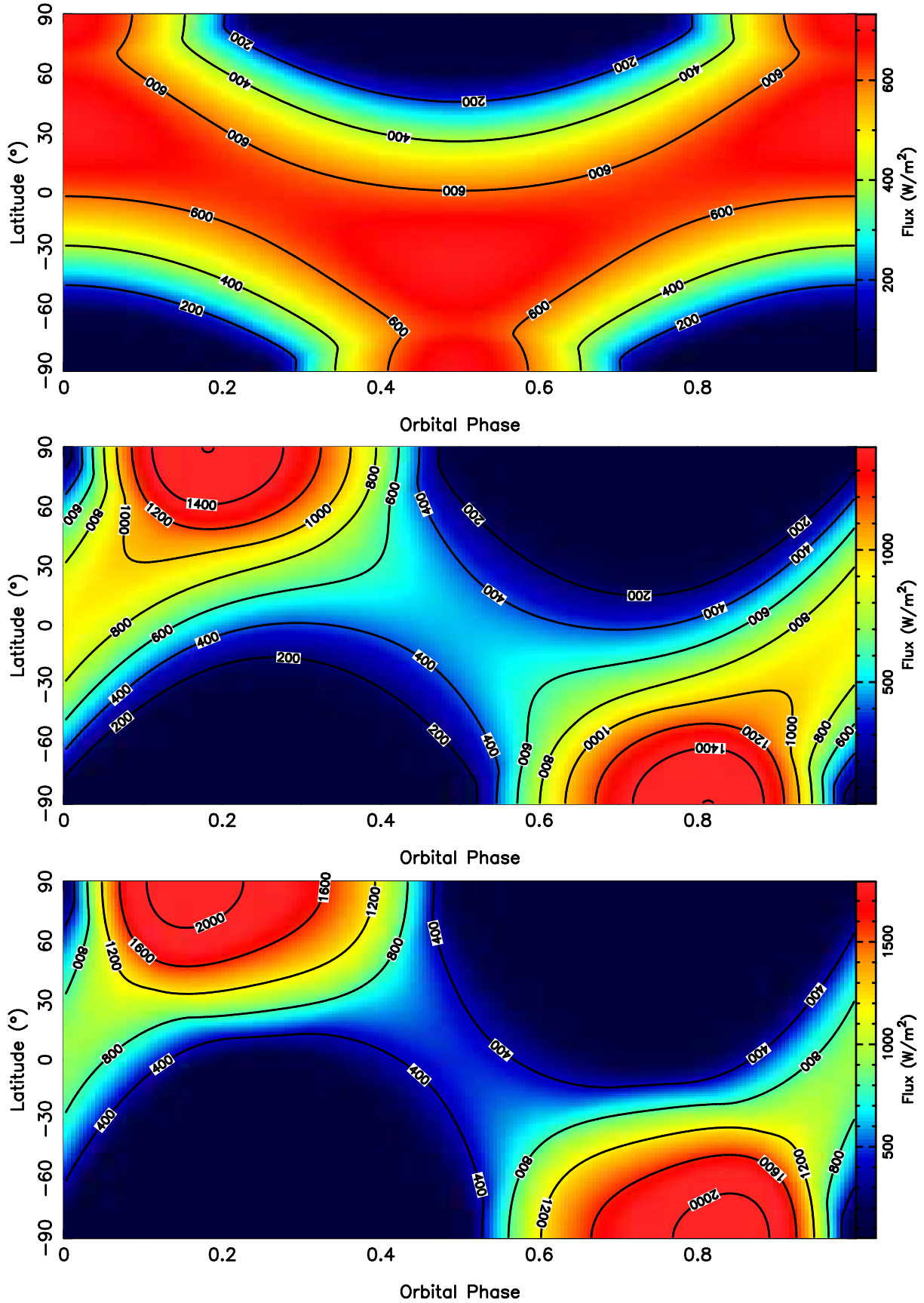


**Figure 7.** Incident flux intensity maps of the planet K2-3 d as a function of latitude and orbital phase, where phase  $\phi = 0.0$  corresponds to periastron passage of the planet. Top:  $e = 0.0$ ,  $\theta = 20^\circ$ ,  $\Delta\phi = 0.0$ . Middle:  $e = 0.162$ ,  $\theta = 50^\circ$ ,  $\Delta\phi = 0.25$ . Bottom:  $e = 0.162$ ,  $\theta = 80^\circ$ ,  $\Delta\phi = 0.25$ .

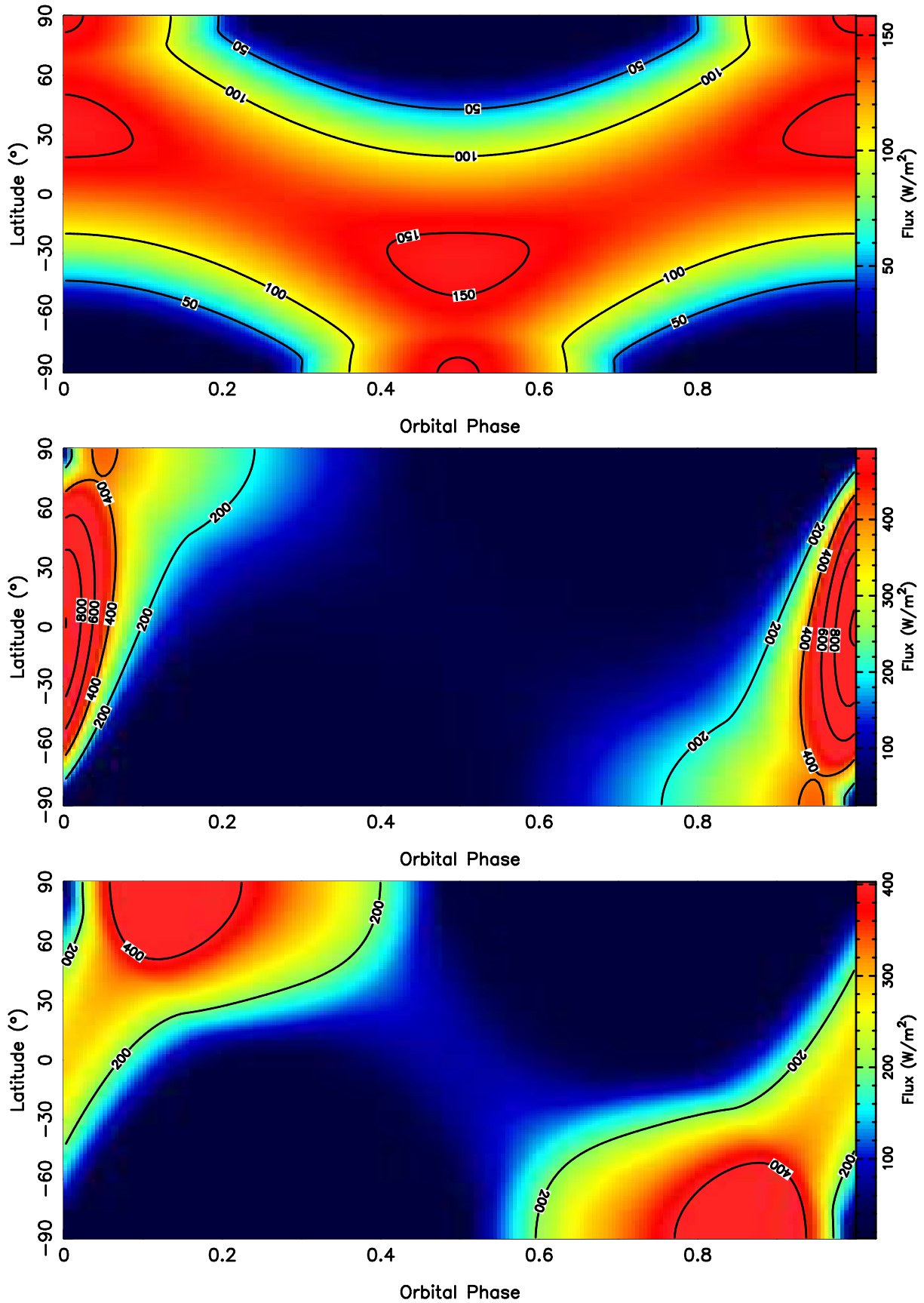


**Figure 8.** Incident flux intensity maps of the planet Kepler-186 f as a function of latitude and orbital phase, where phase  $\phi = 0.0$  corresponds to periastron passage of the planet. Top:  $e = 0.0$ ,  $\theta = 20^\circ$ ,  $\Delta\phi = 0.0$ . Middle:  $e = 0.628$ ,  $\theta = 50^\circ$ ,  $\Delta\phi = 0.25$ . Bottom:  $e = 0.3$ ,  $\theta = 80^\circ$ ,  $\Delta\phi = 0.25$ .

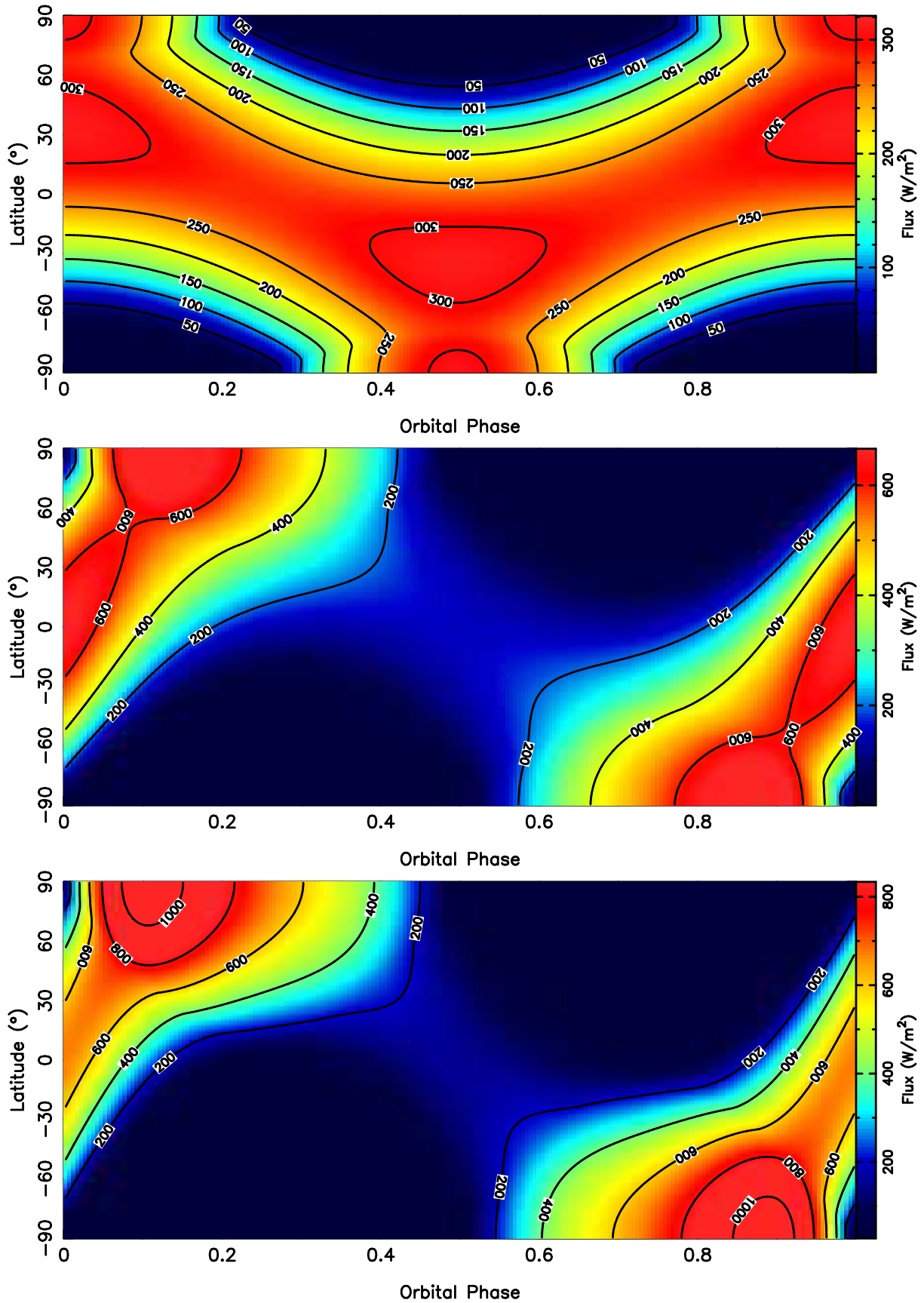


**Figure 9.** Incident flux intensity maps of the planet Proxima Centauri b as a function of latitude and orbital phase, where phase  $\phi = 0.0$  corresponds to periastron passage of the planet. Top:  $e = 0.0$ ,  $\theta = 20^\circ$ ,  $\Delta\phi = 0.0$ . Middle:  $e = 0.35$ ,  $\theta = 50^\circ$ ,  $\Delta\phi = 0.25$ . Bottom:  $e = 0.35$ ,  $\theta = 80^\circ$ ,  $\Delta\phi = 0.25$ .

and thus represents the case where the flux variations match those of the eccentricity at latitude  $\beta = 20^\circ$ . The bottom panel assumes an obliquity of  $\theta = 80^\circ$ . Fully constraining the eccentricity of this planet (and, indeed, of all planets) is clearly critical for developing the needed flux maps to determine climate cycles and potential impacts on surface temperatures.

#### 4. IMPLICATIONS FOR HABITABILITY

The construction of detailed GCMs relies heavily upon many factors, such as the atmospheric composition, temperature-pressure profile, and orbital properties (see references provided in Section 1). With relatively few exceptions, measurements of exoplanet parameters are currently restricted to the mass, radius, and Keplerian orbital properties. Parameters that are inaccessible, at least for terrestrial planets, include the planetary rotation rate and the obliquity of the rotation axis. The influence of rotation rate on atmospheric dynamics for HZ planets has been considered in detail (Yang et al. 2014; Leconte et al. 2015), and it has been shown that the evolution of cloud layers at the substellar point that influence habitable surface conditions is highly sensitive to the rotation period (Kopparapu et al. 2016). It is therefore important to include the diurnal effects that we have incorporated into our flux map models, as described in Section 2.2.

The effect of obliquity on habitable climates is substantial, such as the possibility for HZ planets with large obliquities to experience regular global snowball transitions (Spiegel et al. 2016). For the Earth, the obliquity is stabilized by the Earth’s moon (Laskar et al. 1993; Li & Batygin 2014), without which the obliquity variations would likely have been much more extreme (Laskar & Robutel 1993). Additional simulations for a retrograde-rotating Venus by Barnes et al. (2016) indicate that obliquity variations may have been as low as  $\pm 7^\circ$  over Gyr timescales, implying that massive moons are not necessarily required for obliquity stability. In either case, the obliquity of a particular exoplanet is one that must float as a free parameter in the GCMs that predict surface conditions. A direct measurement of obliquity from seasonal variations in directly detected light will be possible from future missions capable of such measurements. Modeling of these data using current Earth-based observations shows that planetary rotational and obliquity parameters may be inferred from exoplanet imaging photometry (Kane et al. 2015; Kawahara 2016; Schwartz et al. 2016).

A planetary parameter that can be presently measured is the orbital eccentricity. This parameter is most often extracted from the Keplerian orbital solution to RV observations of a bright host star and can also be inferred to a lesser extent from the duration of a planetary

transit (Barnes et al. 2008; Burke 2008). The eccentricities for most of the Kepler HZ planets are largely unknown due to the faintness of the host stars (Kane et al. 2017). In addition, variable eccentricities due to dynamical interactions with other planets can induce Milankovitch cycles with significantly shorter periods than those measured from the Earth (Way & Georgakarakos 2017). The primary purpose of the study described in this work could then be seen as placing constraints on the variable flux from the measurable parameter of eccentricity as a proxy for the presently unknown obliquity of the exoplanet.

#### 5. CONCLUSIONS

Despite the rapid progress in our understanding of terrestrial exoplanets frequency in the HZ, there are many planetary parameters crucial to calculating habitability models that remain beyond our reach. The seasonal variations in incident flux are driven by the orbital eccentricity and the obliquity of the planet’s rotational angular momentum. Within the solar system, Mars is an example of a planet where the obliquity and eccentricity play similar roles in driving the seasonal climate variations. Of the two, eccentricity is currently our only accessible parameter and so it is useful to determine the limits on seasonal variations imposed by the eccentricity that would be matched by a particular obliquity.

In this work, we have calculated the effects of eccentricity and obliquity on incident flux as a function of latitude, and where the flux variations are equivalent for a complete orbital cycle. The two effects largely differ in the Keplerian nature of the eccentricity variations as opposed to the sinusoidal changes in obliquity-induced flux at a given latitude. We selected four case studies of terrestrial planets in the HZ of their host stars where the eccentricity is either measured or we were able to calculate a maximum dynamical eccentricity. These case studies demonstrate where extreme eccentricities and obliquities can dominate the incident flux map and is particularly important in demonstrating the contrast to either the zero eccentricity and/or zero obliquity models. This in turn establishes the importance of constraining eccentricity, as even a relatively small eccentricity ( $e \sim 0.2$ ) can have a large influence on the flux map and climate cycles. Until such time as direct measurements of obliquity can be made, the models presented here will find their utility in constraining obliquity for a given eccentricity and flux map of the planet.

#### ACKNOWLEDGEMENTS

The authors would like to thank Fred Adams, Colin Chandler, and Ravi Kopparapu for useful discussions regarding this work. The authors would also like to thank the anonymous referee, whose comments greatly

improved the quality of the paper. This research has made use of the Habitable Zone Gallery at [hzgallery.org](http://hzgallery.org). This research has also made use of the NASA Exoplanet Archive, which is operated by the California Institute of Technology, under contract with the National Aero-

navitics and Space Administration under the Exoplanet Exploration Program. The results reported herein benefited from collaborations and/or information exchange within NASA's Nexus for Exoplanet System Science (NExSS) research coordination network sponsored by NASA's Science Mission Directorate.

## REFERENCES

- Akeson, R.A., Chen, X., Ciardi, D., et al. 2013, *PASP*, 125, 989
- Almenara, J.M., Astudillo-Defru, N., Bonfils, X., et al. 2015, *A&A*, 581, L7
- Anglada-Escudé, G., Amado, P.J., Barnes, J., et al. 2016, *Nature*, 536, 437
- Armstrong, J.C., Barnes, R., Domagal-Goldman, S., et al. 2014, *AsBio*, 14, 277
- Barnes, R., Raymond, S.N., Jackson, B., Greenberg, R. 2008, *AsBio*, 8, 557
- Barnes, R., Jackson, B., Greenberg, R., Raymond, S.N. 2009, *ApJ*, 700, L30
- Barnes, R., Mullins, K., Goldblatt, C., et al. 2013, *AsBio*, 13, 225
- Barnes, J.W., Quarles, B., Lissauer, J.J., Chambers, J., Hedman, M.M. 2016, *AsBio*, 16, 487
- Barnes, R., Deitrick, R., Luger, R., et al. 2017, *AsBio*, submitted (arXiv:1608.06919)
- Bolmont, E., Raymond, S.N., von Paris, P., et al. 2014, *ApJ*, 793, 3
- Bolmont, E., Libert, A.-S., Leconte, J., Selsis, F. 2016, *A&A*, 591, A106
- Bonfils, X., Lo Curto, G., Correia, A.C.M., et al. 2013, *A&A*, 556, A110
- Burke, C.J. 2008, *ApJ*, 679, 1566
- Crossfield, I.J.M., Petigura, E., Schlieder, J.E., et al. *ApJ*, 804, 10
- Davenport, J.R.A., Kipping, D.M., Sasselov, D., Matthews, J.M., Cameron, C. 2016, *ApJ*, 829, L31
- Dressing, C.D., Spiegel, D.S., Scharf, C.A., Menou, K., Raymond, S.N. 2010, *ApJ*, 721, 1295
- Driscoll, P.E., Barnes, R. 2015, *AsBio*, 15, 739
- Fressin, F., Torres, G., Charbonneau, D., et al. 2013, *ApJ*, 766, 81
- Gladman, B. 1993, *Icarus*, 106, 247
- Howard, A.W. 2013, *Science*, 340, 572
- Howell, S.B., Sobeck, C., Haas, M., et al. 2014, *PASP*, 126, 398
- Kane, S.R., von Braun, K. 2008, *ApJ*, 689, 492
- Kane, S.R., Gelino, D.M. 2012a, *PASP*, 124, 323
- Kane, S.R., Gelino, D.M. 2012b, *AsBio*, 12, 940
- Kane, S.R., Ciardi, D.R., Gelino, D.M., von Braun, K. 2012, *MNRAS*, 425, 757
- Kane, S.R., Domagal-Goldman, S.D., Herman, J.R., Robinson, T.D., Stine, A.R. 2015, *Proceedings of the Comparative Climates of Terrestrial Planets II* (arXiv:1511.03779)
- Kane, S.R., Hill, M.L., Kasting, J.F., et al. 2016, *ApJ*, 830, 1
- Kane, S.R., Gelino, D.M., Turnbull, M.C. 2017, *AJ*, 153, 52
- Kasting, J.F., Whitmire, D.P., Reynolds, R.T. 1993, *Icarus*, 101, 108
- Kaspi, Y., Showman, A.P. 2015, *ApJ*, 804, 60
- Kawahara, H. 2016, *ApJ*, 822, 112
- Kopparapu, R.K., Ramirez, R., Kasting, J.F., et al. 2013, *ApJ*, 765, 131
- Kopparapu, R.K., Ramirez, R.M., SchottelKotte, J., et al. 2014, *ApJ*, 787, L29
- Kopparapu, R.K., Wolf, E.T., Haqq-Misra, J., et al. 2016, *ApJ*, 819, 84
- Laskar, J. 1986, *A&A*, 157, 59
- Laskar, J., Robutel, P. 1993, *Nature*, 361, 608
- Laskar, J., Joutel, F., Robutel, P. 1993, *Nature*, 361, 615
- Leconte, J., Forget, F., Charnay, B., et al. 2013, *A&A*, 554, A69
- Leconte, J., Wu, H., Menou, K., Murray, N. 2015, *Science*, 10, 1126
- Li, G., Batygin, K. 2014, *ApJ*, 790, 69
- Linsemeier, M., Pascale, S., Lucarini, V. 2015, *P&SS*, 105, 43
- Lissauer, J.J., Marcy, G.W., Bryson, S.T., et al. 2014, *ApJ*, 784, 44
- Meadows, V.S., Arney, G.N., Schwieterman, E.W., et al. 2017, *Astrobiology*, submitted (arXiv:1608.08620)
- Petigura, E.A., Marcy, G.W., Howard, A.W. 2013, *ApJ*, 770, 69
- Quintana, E.V., Barclay, T., Raymond, S.N., et al. 2014, *Science*, 344, 277
- Ribas, I., Bolmont, E., Selsis, F., et al. 2016, *A&A*, 596, A111
- Ricker, G.R., Winn, J.N., Vanderspek, R., et al. 2015, *JATIS*, 1, 014003
- Rowe, J.F., Bryson, S.T., Marcy, G.W., et al. 2014, *ApJ*, 784, 45
- Schwartz, J.C., Sekowski, C., Haggard, H.M., Pallé, E., Cowan, N.B. 2016, *MNRAS*, 457, 926
- Sinukoff, E., Howard, A.W., Petigura, E.A., et al. 2016, *ApJ*, 827, 78
- Smith, A.W., Lissauer, J.J. 2009, *Icarus*, 201, 381
- Spiegel, D.S., Menou, K., Scharf, C.A. 2009, *ApJ*, 691, 596
- Sullivan, P.W., Winn, J.N., Berta-Thompson, Z.K., et al. 2015, *ApJ*, 809, 77
- Tuomi, M., Anglada-Escudé, G. 2013, *A&A*, 556, A111
- Turbet, M., Leconte, J., Selsis, F., et al. 2016, *A&A*, 596, A112
- Van Eylen, V., Albrecht, S. 2015, *ApJ*, 808, 126
- Way, M.J., Georgakarakos, N. 2017, *ApJ*, 835, L1
- Weiss, L.M., Marcy, G.W. 2014, *ApJ*, 783, L6
- Williams, D.M., Kasting, J.F. 1997, *Icarus*, 129, 254
- Williams, D.M., Pollard, D. 2002, *IJAsB*, 1, 61
- Williams, D.M., Pollard, D. 2003, *IJAsB*, 2, 1
- Wolf, E., Toon, O.B. 2013, *Astrobiology*, 13, 656
- Wolf, E., Toon, O.B. 2014, *Astrobiology*, 14, 241
- Wordsworth, R., Forget, F., Selsis, F., et al. 2010, *A&A* 522, A22
- Wordsworth, R., Forget, F., Selsis, F., et al. 2011, *ApJ*, 733, L48
- Yang, J., Cowan, N.B., Abbot, D.S. 2013, *ApJ*, 771, L45
- Yang, J., Boué, G., Fabrycky, D., Abbot, D.S. 2014, *ApJ*, 787, L2